Title

Dynamics and Molecular Mechanisms of p53 Transcriptional Activation

Journal

Biochemistry, 57(46)

ISSN

0006-2960

Authors

Offutt, Tavina L
Ieong, Pek U
Demir, Özlem
et al.

Publication Date

2018-11-20

DOI

10.1021/acs.biochem.8b01005

Peer reviewed

HHS Public Access

Author manuscript

Biochemistry. Author manuscript; available in PMC 2020 October 15.

Published in final edited form as:

Biochemistry. 2018 November 20; 57(46): 6528–6537. doi:10.1021/acs.biochem.8b01005.

Dynamics and Molecular Mechanisms of p53 Transcriptional Activation

Tavina L. Offutt, **Pek U Ieong**, **Özlem Demir**, **Rommie E. Amaro***

Department of Chemistry and Biochemistry, University of California, San Diego, 9500 Gilman Drive, La Jolla, CA 92092-0340, United States

Abstract

The “guardian of the genome”, p53, functions as a tumor suppressor that responds to cell stressors such as DNA damage, hypoxia, and tumor formation by inducing cell-cycle arrest, senescence, or apoptosis. Mutation of p53 disrupts its tumor suppressor function, leading to various types of human cancers. One particular mutant, R175H, is a structural mutant that inactivates the DNA damage response pathway and acquires oncogenic functions that promotes both cancer and drug resistance. Our current work aims to understand how p53 wild-type function is disrupted due to the R175H mutation. We use a series of atomistic integrative models built previously from crystal structures of the full-length p53 tetramer bound to DNA and model the R175H mutant using in silico site-directed mutagenesis. Explicitly solvated all-atom molecular dynamics (MD) simulations on wild-type and the R175H mutant p53 reveal insights into how wild-type p53 searches and recognizes DNA, and how this mechanism is disrupted as a result of the R175H mutation. Specifically, our work reveals the optimal quaternary DNA binding mode of the DNA binding domain and shows how this binding mode is altered via symmetry loss as a result of the R175H mutation, indicating a recognition mechanism that is reminiscent of the asymmetry seen in wild type p53 binding to non-specific genomic elements. Altogether our work sheds new light into the hitherto unseen molecular mechanisms governing transcription factor – DNA recognition.

Graphical Abstract

* *Materials & Correspondence* ramaro@ucsd.edu.

Author Contributions

T.L.O. performed the molecular dynamics calculations and analysis and created the figures. P.UI. assisted with analysis and figure preparation. O.D. and R.E.A. directed the project. TLO, PUI, OD, and REA wrote the paper.

SUPPORTING INFORMATION

Additional data (as described in the text) provided in supporting Figures S1–S7 and Tables S1–S3.

Competing Financial Interests

REA is a co-founder of, has equity interest in, and is on the scientific advisory board of Actavalon Inc.

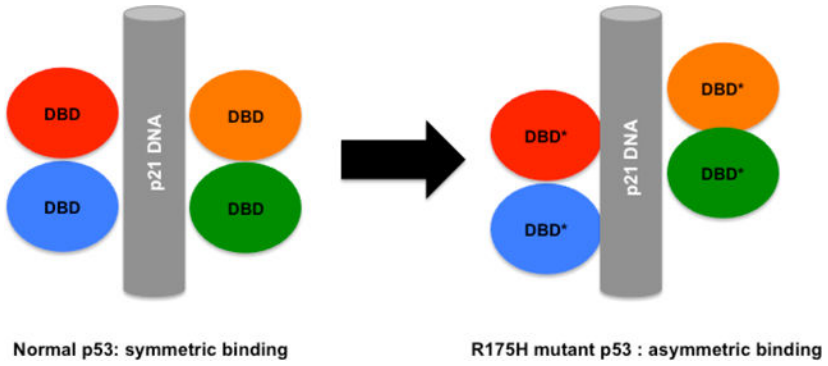

INTRODUCTION

p53, commonly referred to as the “guardian of the genome,” functions as a tumor suppressor. p53 responds to various environmental stressors such as DNA damage, hypoxia, and tumor formation.[1] Once activated, p53 induces cell-cycle arrest, senescence, or apoptosis via either transcriptional or non-transcriptional pathways.[2,3,4] Mutation of p53 disrupts its tumor suppressor function, leading to various types of human cancers, thereby making p53 a major drug target. Our previous computational and experimental studies have revealed stictic acid as a reactivation compound for the R175H p53 mutant.[5] In an effort to expand on this work, we glean insight into how the R175H mutation alters the dynamics of p53 and abrogates its DNA binding abilities. Understanding how full-length p53 (fl-p53) binds DNA and how this binding is disrupted via oncogenic mutations at an atomic level can aid the discovery of novel reactivation compounds.

Fl-p53 contains intrinsically disordered regions and binds DNA as a homotetramer in cells.[6] Fl-p53 comprise of 393 residues that form a N-terminal domain (NTD), proline-rich domain, DNA-binding core domain (DBD), flexible linker region, tetramerization domain (TET), and a C-terminal domain (CTD).[7] The flexible NTD is responsible for activating transcription factors. The proline-rich domain has been implicated in apoptotic activity. The DBD is involved in DNA binding, and the TET domain is crucial for tetramer formation. The CTD is involved both in protein-protein interactions as well as DNA binding.[8,9] There remains controversy in the role of the CTD in fl-p53 DNA binding.[10] Some studies suggest that the CTD serves as a negative regulator by blocking DBD binding to short strands of specific response elements (REs).[11] On the other hand, other studies suggest that the CTD acts as a positive regulator of DNA binding by assisting the DBD in target site recognition in long or circular DNA.[12] Our previous computational studies of the fl-p53 bound to three different DNA response elements captured in atomic detail how the CTDs approach and directly contact the DNA independent of the DNA sequence.[13]

Due to the highly dynamic nature of p53, obtaining an experimental three-dimensional structure of fl-p53 is a challenge. The p53 DBD is the most studied due to its defined secondary and tertiary structural elements, allowing for structural characterization. Also, the DBD contains the majority of oncogenic mutations.[14] While these experimental structures of the DBD has provided useful information about p53 function, it is crucial to model fl-p53 in

order to fully elucidate the DNA-binding mechanism under normal biological conditions. For example, how p53 searches and recognizes specific REs remains unclear. Therefore, the disruption of this search and recognition process due to p53-inactivating mutations is also not well understood.

In an effort to gain insight into the DNA binding mechanism, researchers elucidated a crystal structure of the tetramer of p53 DBD and TET domains with truncated linker regions bound to a short strand of DNA.[15–17] In previous work, we used several other crystal structures of small parts of the missing p53 NTD, CTD and linker regions and molecular modeling to complete this DBD+TET crystal structure and build atomistic integrative models of fl-p53 bound to 3 DNA sequences (two REs and a non-specific DNA), to explore their dynamics via molecular dynamics (MD) simulations.[13] MD-generated ensembles agreed well with previously determined electron microscopy maps and revealed different quaternary binding modes of the fl-p53 bound to different DNA response elements. Our current study expands this work by investigating how oncogenic mutations, specifically the R175H mutation, perturbs the DNA binding interactions of fl-p53.

The R175H mutation results in inactivation of the Mre11/ATM-dependent pathway involved in DNA damage response.[18] This structural mutation also results in abrogation of DNA-binding and perturbs the structure of the p53 DBD.[19, 20] It is also important to note that R175H is a gain-of-function mutant, it not only disrupts normal p53 tumor suppressor function, but also acquires alternative functions necessary for promoting cancer activities.[19] Since this mutation is located at the L2 loop adjacent to the zinc-coordination site, zinc loss is common.[21, 22] Zinc is important for obtaining DNA-binding specificity, and prevents aggregation of the core domain via L2 loop stabilization.[23] Also, in the absence of zinc, the p53 DBD is destabilized by 3.2 kcal/mol.[20] Therefore, we hypothesize that zinc loss exacerbates the effects of the R175H mutation on the DBD. In an effort to monitor this, we use MD simulations to model the p53 DBD R175H mutant with and without zinc.

As a starting structure for the current study, we use the final MD-generated conformation of the atomistic integrative model built previously with available crystal structures of the wild-type fl-p53 tetramer bound to DNA (Figure 1).[13] We model the R175H mutant using *in silico* site-directed mutagenesis (Figure 1). Explicitly solvated all-atom MD simulations are performed in duplicate on the following three fl-p53 systems: (i) wild-type, (ii) R175H mutant with zinc, and (iii) R175H mutant without zinc. Their analysis reveals differences in the conformations of the DNA binding domain and provide insight into how the R175H mutation alone and together with zinc loss destabilizes p53 and abrogates DNA binding.

MATERIALS AND METHODS

Construction of Models

The full-length p53 system was generated as described in previous work.[13] The last frame of the previously simulated wild-type (WT) p53 system bound to the p21 response element was selected for the current study, in which the fl-p53 fully relaxed into a compact structure. All ions and water molecules were removed with the exception of waters within 4 Å of the protein. Three systems were built from the previously simulated p53-p21 system: (i) wild-

type, (ii) R175H with zinc, and (iii) R175H without zinc. The R175H mutation was modeled using *in silico* site-directed mutagenesis in all four monomers. Zinc's tetrahedral geometry was modeled using the dummy cationic atom in the wild-type and R175H mutant with zinc systems.[24] The coordinating cysteine and histidine residues were deprotonated, bearing a negative charge to model zinc-protein coordination. In the R175H mutant without zinc, the correct protonation states for cysteine and histidine residues were determined in the absence of the zinc ion using the online PDB2PQR webserver.[25]

After all three models were built, sodium ions were added to neutralize each system. Using the TIP3P water model,[26] the systems were solvated in a 226 X 193 X 234 box (10 Å in the x-, y-, and z- direction). Each system consisted of ~960,000 atoms and was built using the Amber FF14SB force field.[27]

Molecular Dynamics Simulations

All-atom explicit-solvent molecular dynamics (MD) simulations were performed for the four systems using NAMD2.12.[28] The general MD workflow consisted of three stages: minimization, equilibration, and production. The prepared systems were minimized in five steps as follows: (i) minimization of the protons while restraining the protein, DNA, and solvent for 2000 steps, (ii) minimization of protons, water and ions, while restraining the DNA and protein for 2000 steps, (iii) minimization of the protein and DNA side chains only while restraining the backbone and zinc ion for 2000 steps, (iv) minimization of the zinc coordinating residues only while restraining the non-zinc coordinating protein residues and DNA for 10000 steps, (v) minimization of all atoms in system for 20000 steps. The non-bonded energy was calculated every minimization step. Long-range interactions were calculated using the Particle Mesh Ewald method with a cut-off distance of 10Å.[29] At 8Å, a switching function was applied to improve energy conservation.

The minimized systems were then equilibrated using the NVT ensemble in four steps. All heavy atoms were restrained starting from a weight of 4kcal/mol and reduced gradually to 1kcal/mol. The systems were heated to a temperature of 310K and maintained with Langevin dynamics with a damping coefficient of 5 picoseconds/terahertz. Following equilibration, an NPT ensemble was performed with no positional constraints. A Langevin piston barostat was used to hold the pressure constant at 1 atm with an oscillation period of 100 femtoseconds (fs) and a damping time scale of 50 fs. Two production runs were performed, resulting in a total simulation time of 200ns for each system. Every 5th frame for the simulation was saved and used for analysis.

Principal Components Analysis

The Amber tools cpptraj package was used to perform principal component analysis on the DNA binding domain of p53.[30, 31] The trajectories across all three systems were concatenated and aligned on the α-carbons in the DBD (residues 89 to 291) to remove translation and rotation. The variances of the α-carbon coordinates were determined using the starting conformation for MD as a reference. These variances were used to generate a covariance matrix, A, which was then diagonalized to reveal eigenvectors 1 and 2. Calculation of the covariance matrix A was conducted as follows, yielding the eigenvalues,

λ: $A\mu = \lambda\mu$. These eigenvalues along eigenvectors 1 and 2 were plotted using gnuplot,[32] and used to compare the conformational space of the DBD in the wild-type and mutant p53 MD simulations. Pseudotrajectories were generated to visualize the motion of each eigenvector.

RMSD Clustering Analysis

MD frames unique to each p53 system were extracted and clustered in order to further visualize and analyze PCA results. 'Unique frames' are frames that when projected into PC space, do not overlap with conformations from the other p53 systems. The unique frames were extracted using a python script that selected frames within certain eigenvalue cutoffs (Figure S1), resulting in 650 frames for clustering per system. The extracted frames were aligned to the starting structure for MD on the α-carbons in the DBD. Using the Gromos algorithm,[33] pairwise root-mean-square deviations were calculated and used for clustering the heavy atoms in the L2 and L3 loops L3 loop. The following cutoffs were selected for the L2 and L3 loops respectively: 1.1 Å and 0.9 Å. The top cluster representative for each p53 system was used to visualize differences in the three DBD motifs.

Root-mean-square fluctuation Analysis

The root-mean-square fluctuations (RMSF) of the DBD residues for each monomer were calculated using cpptraj.[30, 31] RMSF is a measure of how a system fluctuates about a well-defined average position. For each p53 system, the MD trajectories were aligned to the starting MD structure using the DBD backbone atoms (N,Cα,C,O) for each monomer, and an average structure was calculated. Using this average structure as the reference, the RMSF of the DBD residues (using only the atoms that make up the backbone) was calculated and plotted using gnuplot.[32]

Volume Calculation

The grab volume between the four DBD monomers that accommodates DNA binding was calculated using POVME 2.0.[34] The visual molecular dynamics (VMD) program[35] was used to generate an inclusion sphere that centered at Cartesian coordinates (128, 135, 115) with a radius of 17 Å, which fully engulfed the volume between the four monomers. A seed was planted in the center of the sphere and extended for 4 Å. POVME 2.0 calculated the grab volume starting from the seed and continued until it reached the inclusion region boundary. The volume was calculated for every MD snapshot, and the volume distribution was plotted as a histogram using the R program.[36]

Solvent Accessible Surface Area Analysis

The solvent accessible surface area (SASA), or the exposed areas of atoms, of the tetramer core domain was measured for each p53 system using cpptraj.[31] The SASA is described as rolling a solvent sphere over the van der Waals surface of a protein. The SASA was calculated in $Å^2$ using the linear combinations of pairwise overlaps (LCPO) algorithm.[37] In the LCPO method, each atom in the protein is represented as a hard sphere. The SASA of each atom sphere was calculated as the difference between the surface area of the atom and the area of atom overlap.

Salt-Bridge Interactions between C-terminal domain and DNA

In order to investigate the C-terminal domain (CTD) - DNA contacts, we measured salt bridges between the positive residues on fl-p53 CTD and the negative DNA phosphate atoms. First, we identified all fl-p53 CTD Lys, Arg, and His residues that came within 5 Å of the DNA at any point of the MD simulation using a tool command language (tcl) script executed in VMD.[35] The trajectories were then loaded into VMD[35] and visual inspection was used to identify salt bridges between the selected Lys/Arg/His residues and DNA phosphate atoms. The distance between the positive nitrogen atoms and negative DNA phosphate oxygen atom throughout the MD trajectory were manually extracted. A python script was used to calculate the percent of the salt-bridge interaction using a distance cutoff of 3.5 Å.

L1/S3 Pocket Open Ratio Calculation

In order to calculate the percentage of the L1/S3 pocket opening, the same distance and angle criteria outlined in Wassman *et al.*[5] was used. First, we used cpptraj[31] to define the four distances and one dihedral angle associated with the L1/S3 pocket that served as input for the calculation. Next, using an in-house python script, the frames that satisfied the distance and angle criteria were identified, and used in calculating the percentage of the time the pocket was open.

Data Availability

The atomic coordinates of the final MD frames of each system are available in pdb format at modelarchive.org.

RESULTS

We performed 200 ns of MD simulations for all three wild-type and R175H mutant fl-p53 systems, resulting in a total simulation time of 600 ns (Table S1). We explored how the R175H structural mutation with and without zinc changes the dynamic behavior of fl-p53 both globally and locally. Ultimately, we glean insight into how these changes in flexibility destabilizes the DBD and alters DNA binding in the p53 R175H mutant.

Unique Binding Modes of Wild-type and R175H p53 DBD Tetramer to DNA

In order to investigate the effect of p53 structural perturbations (R175H mutation and zinc loss) on DNA binding, the Cartesian coordinates for each atom in the DBD over time were reduced to 2D principal component (PC) space. This reduction parsed the motion with the largest variance or the most descriptive motion of the DBD that was not apparent from simple visualization of the MD trajectories.

When projected onto 2D principal component (PC) space, the DBD tetramer for each fl-p53 system differs in DNA binding modes (Figure 2 and S1). Interestingly, the first principal motion (PC1) described a global conformational change going from an asymmetric binding mode (low PC1) where monomers A and D are pushed away from the DNA and monomers B and C are close together to a symmetric binding mode (high PC1) in which all four monomers are in close proximity to DNA (Figure 2a). In our simulations, the wild-type and

R175H with zinc tetramer systems solely sampled high PC1 values while the R175H without zinc system mostly sampled low PC1 values. This suggests zinc loss is far more important in DNA binding failure of p53 than the R175H mutation itself.

In addition to the change in symmetry of the DBD monomers, the PC1 motion also revealed differences in the DNA grab volume, which is the space in between the four p53 DBD monomers that accommodates the DNA. This volume is largest for R175H with zinc, smaller for wild-type, and smallest for R175H without zinc (Figure 2b). The large difference in the DNA grab volume is due to changes in the L2 loop conformations of monomers B and C. The grab volume is small in R175H without zinc system, as the L2 loops in these two monomers are stabilized via multiple hydrogen bonding interactions, where the distance between the donor and acceptor heavy atoms was no more than 3.0 Å (Table 1). In the wild-type system, one hydrogen bond is seen in the wild type p53 system in only 0.05% of the trajectory (Table 1), and no hydrogen bonds are observed in the R175H with zinc system. There are also differences seen in a salt-bridge near the mutation site in the L2 loop between residues E180 and R174 (Figure S2). In the wild-type system, this salt-bridge is persistent throughout the simulation, where it occurs 66.4±5.8% of the time across both MD copies. However, in the mutant systems, this salt-bridge is less persistent with one exception. In the R175H with zinc system, this salt bridge forms 43.8±1.2% of the time across both MD copies. For R175H without zinc, this salt-bridge only forms 47.9±43.8% of the time across both MD copies, it should be noted that the large standard deviation for the R175H without zinc system is due to the fact that the disrupted salt-bridge is seen in only one MD copy.

PC2 is similar to PC1, but shows more local motion of the global symmetry motion seen in PC1. In PC2, monomers A and D rotate in opposite directions (Movie S1 and Figure S1). Similar to the PC1 motion, monomers B and C move closer to each other going from low PC2 to high PC2.

Each fl-p53 system sampled unique conformations not sampled by the other two systems (yellow box in Figure S1). In order to further visualize the differences in these unique conformations, root-mean-square deviation (RMSD) clustering was performed on the L2 and L3 loops separately since they embrace the R175H mutation site, and the L2 loop stabilizes the L3 loop. The representative frame of the most-populated cluster for each system was compared.

When clustered with respect to the L2 loop, the differences in the L2 loop conformations for the three systems' representative frames were in line with the PC1 motion, in which the L2 loops of monomers B and C formed direct contacts in the R175H without zinc system unlike the other two systems (Figure 3a).

When clustered with respect to the L3 loop, the representative frames for the three systems differ in the conformation of the R248 residue, a crucial DNA contact, in monomer C (Figure 3b). In the wild-type representative frame, R248 extends directly into the DNA minor groove similar to the crystal structure (PDB 1TSR). In the R175H with zinc representative frame, R248 adopts an alternate conformation that does not intercalate into the DNA minor groove. In the R175H without zinc representative frame, R248 remains on

the surface, but is completely flipped out of the minor groove. The conformation of R248 in monomers A, B, and D in the top cluster representative is similar across all three fl-p53 systems.

Comparison of atomic fluctuations within the DBD

Increased fluctuations of motifs within the DBD are seen for the R175H with zinc system in monomers B, C, and D (Figure S3). For the two inner monomers, B and C, the L2 and L3 loops are more dynamic in the R175H with zinc system compared to the wild-type system. Among the outer monomers, monomer D becomes more flexible at the loop between beta strands 7 and 8 (S7/S8 loop) in the R175H with zinc system. Surprisingly, the dynamic behavior of monomer A is similar in the R175H with zinc and wild-type systems.

An increase in atomic fluctuations is seen also in the R175H without zinc system compared to the wild-type system (Figure S4). This difference in flexibility is seen in the L2 and L3 loops for the inner monomers B and C. Interestingly, the L1 loop and H2 helix in monomer C also show greater fluctuations in the R175H without zinc system. Among the outer monomers, monomer D also shows increased flexibility at the L2 and L3 loops. In monomer A, the only RMSF variation is observed at the S7/S8 loop.

While we don't see more flexibility in the R175H mutant systems across the entire tetramer DBDs or even an entire monomer, we do observe increased fluctuations local to the R175H mutation site in monomers B, C, and D. Interestingly, fluctuations distal to the mutation site are also observed as seen in monomer D in R175H with zinc system and monomer C in R175H without zinc system.

Comparison of the solvent accessible surface area of the DBD Tetramer

Protein fluorescence experimental studies have revealed differences in fluorescence spectra between wild-type and mutant p53, which is attributed to increased solvent accessible surface area (SASA) in mutants.[20] In terms of the SASA for the entire DBD tetramers, both R175H mutant systems have higher values than wild-type p53 as expected (Figure S5). Next, we focused on determining the solvent exposure of only the mutant epitope residues (residues 213–217) that are known to bind the Pab240 antibody that selectively recognizes the mutant conformation of p53 but not wild-type p53.[38] These residues are buried in the wild-type, and become more solvent exposed for antibody binding in p53 mutants.

Similar to the entire DBD tetramer, when we focus only on the mutant epitopes, the average SASA is higher for both R175H mutant systems compared to the wild-type (Figure S5). Taken together, the SASA results for the entire DBD tetramer and the epitope regions corroborate experimental evidence suggesting that the R175H mutant form has increased solvent accessibility compared to the wild-type.

Comparison of C-terminal domain contacts with DNA

Previous computational models[13] have shown that the CTDs form direct DNA contacts regardless of the DNA response element. In addition, Friedler *et al.* suggest these CTD-DNA contacts are likely due to low affinity electrostatic interactions between positively charged

residues in the CTD and the negatively charged DNA phosphate backbone.[39] We explore if these CTD-DNA contacts change as a result of the R175H mutation. Our MD simulations revealed there are in fact differences in the CTD-DNA contacts, with the largest change seen in the R175H without zinc system (Table S2). In all three fl-p53 systems, all the positively charged CTD residues' (Lys, His, Arg) interactions with the negatively charged DNA phosphates were monitored. In monomer C, the CTD forms contacts with the DNA throughout the entire simulation across all three fl-p53 systems. These contacts are transient, in which the positively charged CTD residues continuously change the phosphate groups they contact. It should be noted that the initial starting structure for the MD simulations across all three fl-p53 systems already had this CTD-DNA contact in monomer C while the CTDs in the other monomers were far away from the DNA. In the wild-type and R175H with zinc systems, the CTDs in monomers A and D move closer to and form DNA contacts. Remarkably, other than the CTD in monomer C, the R175H without zinc mutant failed to form additional CTD-DNA contacts, suggesting that the loss of zinc due to the R175H mutation disrupts CTD-DNA interactions.

Next, we closely monitored if any specific positively charged CTD residues were responsible for the transient salt-bridge interactions with DNA, and identified four residues (Figures 4a and S6). A cutoff value of 600 was chosen since this is half of the maximum number of CTD-DNA salt-bridge contacts. For both wild-type and R175H with zinc systems, CTD residues K370, R379, K381, and K382 form at least 600 DNA contacts. For R175H without zinc system, only residues H368 and R379 engage in at least 600 DNA contacts. Interestingly, residues K370, K381, and K382 have reduced DNA contacts when compared to wild-type and R175H with zinc systems. In terms of the average across all three p53 systems, K370, R379, K381, and K382 form at least half of the maximum contacts (Figures 4a and S6).

We also identified the DNA residues that the CTD residues interact with, and found that salt bridges formed both inside and outside the response element (Figures 4b and S7). Across all three p53 systems, only a few contacts are made within the response element (residues 1599–1602, 1665, 1681–1684) (black box in Figures 4b and S7). Majority of the CTD-DNA interactions occur outside the DNA response element, interacting with DNA nucleotides up 10 base pairs to the right and 14 base pairs to the left from the response element (Figure 4b). The CTD searches furthest along the DNA in the R175H mutant systems (Figure S7). These results are in agreement with NMR models that show that the CTD interacts with DNA outside the response element region.[40]

L1/S3 Pocket Opening

In an earlier study, MD simulations of wild-type and various p53 mutant DBD monomers revealed a druggable L1/S3 pocket.[5] Using several geometric criteria as a filter for determining the pocket-open state, the pocket was found to be open only about 6% of the time in a 30 ns simulation. Virtual screens targeting the open MD-generated conformations of L1/S3 pocket revealed a novel reactivation compound for p53 R175H mutant. We then inquired the dynamics of the L1/S3 pocket in a larger fl-p53 tetramer system bound to various DNA sequences, which revealed the L1/S3 pocket dynamics depend mostly on the

L1 loop conformation (which is dictated by being an inner or an outer monomer in its DNA interaction) in p53, which can stay open as much as 99% of the simulation time.[13]

In the current study, we compute the L1/S3 pocket dynamics of the p53 R175H mutants under normal physiological conditions using the same geometric criteria outlined in Ref 4 (Table S3). For the inner monomers B and C, the L1/S3 pocket is open only 4% to 13% of the time for wild-type system, 7% to 24% for R175H with zinc system, and 4% to 15% for R175H without zinc system. The pocket is open for majority of the simulation time in the outer monomers, A and D, for all three systems with two exceptions (24% to 95% for wild-type system, 67% to 96% for R175H with zinc system, and 21% to 96% for R175H without zinc system). These results show that in the fl-p53 R175H mutants, the L1/S3 pocket is open and available for reactivation molecules to bind in restoring p53 wild-type function.

DISCUSSION

We report here three different integrative atomistic models of the wild-type and R175H mutant fl-p53 tetramer bound to the p21 response element and their dynamics via MD simulations. Experimental studies have shown that the R175H mutation accelerates the rate of zinc loss in the DBD.[21, 22] As there are no available experimental structures of the R175H mutant even of the DBD due to the denaturing effect of the mutation, we generate a computational model the R175H mutation in both the presence and absence of zinc. The dynamics of the R175H mutation in the fl-p53 and its effects on DNA binding have not been explored.

R175H Mutation Shifts the DBD Quaternary Binding Mode Similar to Wild-type p53 Binding Mode to Non-specific DNA

The DBD quaternary binding modes revealed in the current work are closely related to the differential quaternary binding modes we found earlier for fl-p53 binding to three different DNA response elements (p21 RE, puma RE, and non-specific DNA) (Figure 5).[13] The binding affinity for fl-p53 for known REs, p21 and puma for example, are an order of magnitude lower than the K_D values of non-specific DNAs under physiological conditions.[41]

The PC1 motion revealed in the current work is the same global motion that was seen as PC2 in our previous studies of fl-p53 bound to 3 different DNA sequences.[13] In the previous work, the p21-bound wild-type p53 tetramer system sampled only high PC2 values corresponding to a symmetric binding mode. The same binding mode is seen in our current wild type simulations (Figure 2). The only difference between the p21-bound p53 tetramer in the previous work and our current p21-bound p53 tetramer system (referred to as wild-type) is the starting conformation for the MD simulations. In the previous model, the fl-p53 started from a conformation where the CTDs and NTDs were extended.[13] The current wild-type system simulations started from the more compact relaxed fl-p53 structure. The additional MD sampling in this study corroborates the results from previous study, which indicated a symmetric DBD tetramer binding mode for wild-type p53 binding to known DNA response elements.

The PC motions of the quaternary binding modes of the mutant fl-p53 systems clearly show the R175H mutation disrupts DNA binding. In the previous computational study, the p53 tetramer bound to nonspecific-DNA solely sampled an asymmetric binding mode.[13] Remarkably, the R175H mutant without zinc system mostly samples this same asymmetric quaternary binding mode.

As for the DNA grab volume change revealed in the PC motions, there are both similarities and differences when compared to our previous computational study (Figure 2). The small grab volume seen in the R175H without zinc system is comparable to that seen for the non-specific DNA bound DBD tetramer. Also, as seen in the previous work, the wild-type system does have a larger DNA grab volume (ranging between 8000 and 9000 $Å^3$) to accommodate the DNA than the DBD tetramer bound to non-specific DNA and the R175H without zinc mutant. Surprisingly, the R175H with zinc system has the largest DNA grab volume, which may be too loose to bind the DNA tightly.

Increased Local and Global Flexibility in the R175H Mutant DBD Disrupt Crucial DBD-DNA Contacts

The DBD motifs with increased flexibility in the R175H mutant systems are also regions known to contact DNA either directly or indirectly (Figures S3 and S4). In the L2 loop of various wild-type p53 crystal structures, R175 forms a salt-bridge with D184, helping the L2 loop stabilization.[42, 43] The R175H mutation disrupts this R175-D184 salt-bridge. We also identify another salt bridge, E180-R174, that is persistent in the wild-type simulations and disrupted in both R175H mutant system simulations. Disruptions of these two salt-bridges in the mutant p53 increase the flexibility of the L2 loop (Figures S3 and S4). The higher flexibility of the L2 loop destabilizes the L3 loop, which directly contacts the DNA via two residues, S241 and R248. While the DNA contact of S241 stays intact in all systems, the R248-DNA contact is effected by the mutation, the R248 intercalate the DNA minor groove in the wild-type system but doesn't in the R175H mutant system (Figure 3b). R248 is known to play a critical role in DNA binding and it is the most frequently mutated p53 residue in human cancers.[44–46] Therefore, the loss of this DNA contact may impede DNA binding of the R175H mutant. Even though this difference in R248 conformation is only observed in one DBD monomer (monomer C), experimental studies have shown that a heterotetramer with only one mutant p53 monomer is enough to shift the wild-type p53 to resemble a mutant conformation and disrupt DNA binding.[47–49] In addition to the increased flexibility of motifs local to the R175H mutation site, it is noteworthy that we see the effect of the mutation on long-range motions such as the H2 helix, L1 loop, and S7/S8 loop, especially in quite short MD sampling (Figures S3 and S4). With our limited computational sampling, we are already beginning to see the destabilization of the DBD both locally at the R175H mutation site and globally.

R175H Mutation and Zinc Loss Together Disrupt C-terminal interactions with DNA

The role of the CTD in DNA binding remains controversial. Previous studies have suggested three possible theories as to how the CTD of p53 regulates sequence-specific DNA binding.[10] One theory suggests that the DBD tetramers only bind the DNA when it undergoes a conformational change induced by chemical modification (acetylation or phosphorylation)

or protein binding of the C-terminus. Another hypothesis suggests that CTD binding to the DNA prevents the DBD tetramers from binding, and chemical modification of CTD disrupts DNA binding, thereby allowing the DBD to bind DNA. Both of these theories suggest that the CTD functions as a negative regulator for p53 binding. The third theory implies that the CTD acts as a positive regulator for DBD binding. Our previous and current studies support the latest theory.

In our simulations, we see transient CTD interactions with DNA phosphates (Table S2). These observations are in agreement with experimental studies that reveal that the CTD forms sequence-independent contacts with DNA.[40, 50–52] It is particularly interesting that the CTD monomers (A and D) that were extended far away from the DNA move closer to the DNA and form direct contacts in wild-type and R175H with zinc simulations centered on CTD residues K370, R379, K381, and K382. Among these, K381 and K382 were implicated in CTD-DNA contacts in an NMR study.[40, 53] This direct CTD-DNA contact was also seen in our previous computational models where the CTDs started from an extended conformation far from the DNA, in every simulation regardless of the DNA response element, the CTD approached and directly contacted the DNA, suggesting that the CTD assists the DBD in binding DNA.[13] In the R175H without zinc system, the only CTD monomer that forms DNA contacts is monomer C, which was already in contact initially. Unlike the other 2 systems, no other CTDs approach DNA to form contacts, and reduced DNA contacts are seen for residues K370, K381, and K382. Taken together, the combination of R175H mutation and zinc loss disrupt CTD-DNA contacts.

CONCLUSION

In this study, we used MD simulations to explore the effects of the R175H cancer mutation on the dynamic characteristics of fl-p53, and how these changes disrupt DNA binding. Results reveal increased flexibility of motifs within the DBD both local and distal to the R175H mutation site. Interestingly, these motifs are regions that form important DNA contacts. The accelerated dynamics disrupt the DBDs from adopting an optimal DNA binding mode and alter the frequency of CTD-DNA contacts. Taken together, our mutant models in the current work and previous models with fl-p53 bound to different DNA response elements allow us to glean insight into the DNA search and recognition mechanism even with limited MD sampling. In wild-type p53, the DBD adopts a symmetric binding mode around the DNA, and three Lys residues and one Arg residue of the CTDs aid in DNA binding by forming transient non-specific contacts with the DNA mostly outside the response element region. When p53 has the R175H cancer mutation together with zinc loss, the DBDs shift to an asymmetric binding mode around the DNA, and the CTD-DNA contacts are disrupted. The results of our computational models support our hypothesis that zinc loss exacerbates the effects of the R175H mutation in destabilizing the DBD and abrogating DNA binding.

Supplementary Material

Refer to Web version on PubMed Central for supplementary material.

ACKNOWLEDGEMENTS

The authors thank Jamie Schiffer for review of the manuscript. This work was funded by the NIH, under DP2-OD007237 and P41-GM103426, and by the NSF under CHE060073N, to REA. We give special thanks to the computing team at the Texas Advanced Computing Cluster (TACC) for early access to Stampede2.

REFERENCES

1. Freed-Pastor WA, Prives C (2012) Mutant p53: one name, many proteins, Genes Dev 26, 1268–1286. [PubMed: 22713868]
2. Green DR, Kroemer G (2009) Cytoplasmic functions of the tumour suppressor p53, Nature 458, 1127–1130. [PubMed: 19407794]
3. Valente LJ, Gray DH, Michalak EM, Pinon-Hofbauer J, Egle A, Scott CL, Janic A, Strasser A (2013) p53 Efficiently Suppresses Tumor Development in the Complete Absence of Its Cell-Cycle Inhibitory and Proapoptotic Effectors p21, Puma, and Noxa, Cell Rep 3, 1339–1345. [PubMed: 23665218]
4. Li TY, Kon N, Jiang L, Tan MJ, Ludwig T, Zhao YM, Baer R, Gu W (2012) Tumor Suppression in the Absence of p53-Mediated Cell-Cycle Arrest, Apoptosis, and Senescence, Cell 149, 1269–1283. [PubMed: 22682249]
5. Wassman CD, Baronio R, Demir O, Wallentine BD, Chen CK, Hall LV, Salehi F, Lin DW, Chung BP, Hatfield GW, Richard Chamberlin A, Luecke H, Lathrop RH, Kaiser P, Amaro RE (2013) Computational identification of a transiently open L1/S3 pocket for reactivation of mutant p53, Nat. Commun. 4, 14071415.
6. Tidow H, Melero R, Mylonas E, Freund SM, Grossmann JG, Carazo JM, Svergun DI, Valle M, Fersht AR (2007) Quaternary structures of tumor suppressor p53 and a specific p53 DNA complex, Proc. Natl. Acad. Sci. 104, 12324–12329. [PubMed: 17620598]
7. Hupp TR (1999) Regulation of p53 protein function through alterations in protein-folding pathways, Cell Mol. Life Sci. 55, 88–95. [PubMed: 10065154]
8. Kannan S, Lane D, Verma C (2016) Long range recognition and selection in IDPs: the interactions of the C-terminus of p53, Sci. Rep. 6, 23750–23762. [PubMed: 27030593]
9. Joerger AC, Fersht AR (2010) The Tumor Suppressor p53: From Structures to Drug Discovery, Cold Spring Harb Perspect. Biol 2, a000919.
10. Ahn J, Prives C (2001) The C-terminus of p53: the more you learn the less you know, Nat. Struct. Bio. 8, 730–732. [PubMed: 11524665]
11. Hupp TR, Meek DW, Midgley CA, Lane DP (1992) Regulation of the Specific DNA-Binding Function of P53, Cell 71, 875–886. [PubMed: 1423635]
12. McKinney K, Mattia M, Gottifredi V, Prives C (2004) p53 linear diffusion along DNA requires its C terminus, Mol. Cell 16, 413–424. [PubMed: 15525514]
13. Demir O, Ieong PU, Amaro RE (2017) Full-length p53 tetramer bound to DNA and its quaternary dynamics, Oncogene 36, 1451–1460. [PubMed: 27641333]
14. Lukman S, Lane DP, Verma CS (2013) Mapping the Structural and Dynamical Features of Multiple p53 DNA Binding Domains: Insights into Loop 1 Intrinsic Dynamics, Plos One 8, e80221.
15. Emamzadah S, Tropia L, Halazonetis TD (2011) Crystal structure of a multidomain human p53 tetramer bound to the natural CDKN1A (p21) p53-response element, Mol. Cancer Res. : MCR 9, 1493–1499. [PubMed: 21933903]
16. Petty TJ, Emamzadah S, Costantino L, Petkova I, Stavridi ES, Saven JG, Vauthey E, Halazonetis TD (2011) An induced fit mechanism regulates p53 DNA binding kinetics to confer sequence specificity, EMBO J. 30, 2167–2176. [PubMed: 21522129]
17. Emamzadah S, Tropia L, Vincenti I, Falquet B, Halazonetis TD (2014) Reversal of the DNA-binding-induced loop L1 conformational switch in an engineered human p53 protein, J. Mol. Biol. 426, 936–944. [PubMed: 24374182]
18. Xu Y (2006) DNA damage: a trigger of innate immunity but a requirement for adaptive immune homestasis, Nat. Rev. Immunol. 6, 261–270. [PubMed: 16498454]

19. Sigal A, Rotter V (2000) Oncogenic mutations of the p53 tumor suppressor: the demons of the guardian of the genome, Cancer Res 60, 6788–6793. [PubMed: 11156366]
20. B Bullock AN, Henckel J, Fersht AR (2000) Quantitative analysis of residual folding and DNA binding in mutant p53 core domain: definition of mutant states for rescue in cancer therapy, Oncogene 19, 1245–1256. [PubMed: 10713666]
21. Butler JS, Loh SN (2003) Structure, function, and aggregation of the zinc-free form of the p53 DNA binding domain, Biochemistry 42, 2396–2403. [PubMed: 12600206]
22. Joerger AC, Fersht AR (2007) Structure-function-rescue: the diverse nature of common p53 cancer mutants, Oncogene 26, 2226–2242. [PubMed: 17401432]
23. Duan J, Nilsson L (2006) Effect of Zn2+ on DNA recognition and stability of the p53 DNA-binding domain, Biochemistry 45, 7483–7492. [PubMed: 16768444]
24. Pang YP (1999) Novel zinc protein molecular dynamics simulations: Steps toward antiangiogenesis for cancer treatment, J Mol Model 5, 196–202.
25. Dolinsky TJ, Nielsen JE, McCammon JA, Baker NA (2004) PDB2PQR: an automated pipeline for the setup, execution, and analysis of Poisson-Boltzmann electrostatics calculation, Nucleic Acids Res. 32, W665–W667. [PubMed: 15215472]
26. Jorgensen WL, Chandrasekhar J, Madura JD (1983) Comparison of simple potential functions for simulating liquid water, J Chem Phys 79, 926–935.
27. Maier JA, Martinez C, Kasavajhala K, Wickstrom L, Hauser KE (2015) Simmerling, C., ff14SB: Improving the Accuracy of Protein Side Chain and Backbone Parameters from ff99SB, J. Chem. Theory Comput. 11, 3696–3713. [PubMed: 26574453]
28. Phillips JC, Braun R, Wang W, Gumbart J, Tajkhorshid E, Villa E, Chipot C, Skeel RD, Kale L, Schulten K (2005) Scalable molecular dynamics with NAMD, J. Comput. Chem. 26, 1781–1802. [PubMed: 16222654]
29. Darden T, Perera L, Li L, Pedersen L (1999) New tricks for modelers from the crystallography toolkit: the particle mesh Ewald algorithm and its use in nucleic acid simulations, Structure 7, R55–R60. [PubMed: 10368306]
30. Case DA, Berryman JT, Berryman Betz RM, Cerutti DS, Cheatham TE III, Darden TA, Duke RE, Giese TJ, Gohlke H, Goetz AW, Homeyer N, Izadi S, Janowski P, Kaus J, Kovalenko A, Lee TS, LeGrand S, Li P, Luchko T, Luo R, Madej B, Merz KM, Monard G, Needham P, Nguyen H, Nguyen HT, Omelyan I, Onufriev A, Roe DR, Roitberg A, Salomon-Ferrer R, Simmerling CL, Smith W, Swails J, Walker RC, Wang J, Wolf RM, Wu X, York DM and Kollman PA (2015) AMBER 2015. University of California, San Francisco.
31. Roe DR, Cheatham TE (2013) 3rd, PTRAJ and CPPTRAJ: Software for Processing and Analysis of Molecular Dynamics Trajectory Data, J. Chem. Theory Comput. 9, 3084–3095. [PubMed: 26583988]
32. Janert PK (2010) Gnuplot in action : understanding data with graphs. Manning Publications: Greenwich, Conn, 2010, p xxxi, 360 pages.
33. Van Der Spoel D, Lindahl E, Hess B, Groenhof G, Mark AE, Berendsen HJ (2005) GROMACS: fast, flexible, and free, J. Comput. Chem. 26, 1701–1718. [PubMed: 16211538]
34. Durrant JD, Votapka L, Sorensen J, Amaro RE (2014) POVME 2.0: An Enhanced Tool for Determining Pocket Shape and Volume Characteristics, J. Chem. Theory Comput. 10, 5047–5056. [PubMed: 25400521]
35. Humphrey W, Dalke A, Schulten K (1996) VMD: visual molecular dynamics, J. Mol. Graphics 14, 33–38.
36. Wickham H, Ggplot2 elegant graphs for data analysis In Use R, Springer: New York, 2009, pp viii, 212 pages.
37. Weiser J, Shenkin PS, Still WC (1999) Approximate atomic surfaces from linear combinations of pairwise overlaps (LCPO), J. Comput. Chem. 20, 217–230.
38. Gannon JV, Greaves R, Iggo R, Lane DP (1990) Activating mutations in p53 produce a common conformational effect. A monoclonal antibody specific for the mutant form, EMBO J. 9, 1595–1602. [PubMed: 1691710]

39. Friedler A, Veprintsev DB, Freund SM, von Glos KI, Fersht AR (2005) Modulation of binding of DNA to the C-terminal domain of p53 by acetylation, Structure 13, 629–636. [PubMed: 15837201]
40. Krois AS (2017) Versatility through Flexibility - p53 and Intrinsic Disorder. Scripps Research Institute, La Jolla, CA.
41. Weinberg RL, Veprintsev DB, Fersht AR (2004) Cooperative binding of tetrameric p53 to DNA, J. Mol. Biol. 341, 1145–1159. [PubMed: 15321712]
42. Kitayner M, Rozenberg H, Kessler N, Rabinovich D, Shaulov L, Haran TE, Shakked Z (2006) Structural basis of DNA recognition by p53 tetramers, Mol Cell 22, 741–753. [PubMed: 16793544]
43. Wang Y, Rosengarth A, Luecke H (2007) Structure of the human p53 core domain in the absence of DNA, Acta Crystallogr. Sect D: Biol. Crystallogr. 63, 276–281. [PubMed: 17327663]
44. Takahashi T, Nau MM, Chiba I, Birrer MJ, Rosenberg RK, Vinocour M, Levitt M, Pass H, Gazdar AF, Minna JD (1989) p53: a frequent target for genetic abnormalities in lung cancer, Science 246, 491–494. [PubMed: 2554494]
45. Hollstein M, Sidransky D, Vogelstein B, Harris CC (1991) p53 mutations in human cancers, Science 253, 49–53. [PubMed: 1905840]
46. Nigro JM, Baker SJ, Preisinger AC, Jessup JM, Hostetter R, Cleary K, Bigner SH, Davidson N, Baylin S, Devilee P, et al. (1989) Mutations in the p53 gene occur in diverse human tumour types, Nature 342, 705–708. [PubMed: 2531845]
47. Chene P (1998) In vitro analysis of the dominant negative effect of p53 mutants, J. Mol. Biol. 281, 205–209. [PubMed: 9698540]
48. Milner J, Medcalf EA (1991) Cotranslation of activated mutant p53 with wild type drives the wild-type p53 protein into the mutant conformation, Cell 65, 765–774. [PubMed: 2040013]
49. Milner J, Medcalf EA, Cook AC (1991) Tumor suppressor p53: analysis of wild-type and mutant p53 complexes, Mol Cell Biol 11, 12–19. [PubMed: 1986215]
50. Halazonetis TD, Kandil AN (1993) Conformational shifts propagate from the oligomerization domain of p53 to its tetrameric DNA binding domain and restore DNA binding to select p53 mutants, EMBO J. 12, 5057–5064. [PubMed: 8262048]
51. Oberosler P, Hloch P, Ramsperger U, Stahl H (1993) p53-catalyzed annealing of complementary single-stranded nucleic acids, EMBO J. 12, 2389–2396. [PubMed: 7685274]
52. Wu WJ, Kakehi Y, Habuchi T, Kinoshita H, Ogawa O, Terachi T, Huang CH, Chiang CP, Yoshida O (1995) Allelic frequency of p53 gene codon 72 polymorphism in urologic cancers, Jpn. J. Cancer Res. 86, 730–736. [PubMed: 7559095]
53. Weinberg RL, Freund SM, Veprintsev DB, Bycroft M, Fersht AR (2004) Regulation of DNA binding of p53 by its C-terminal domain, J. Mol. Biol. 342, 801–811. [PubMed: 15342238]

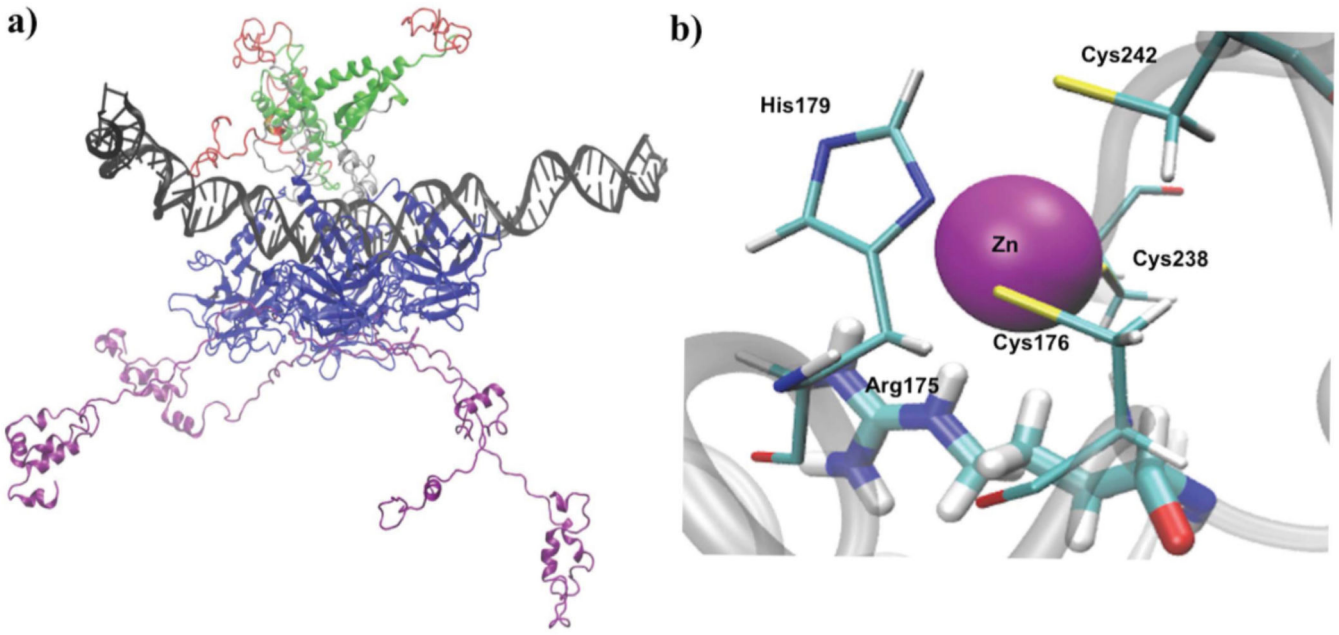

Figure 1.

Full-length p53 System. The fl-p53 bound to DNA is shown, where the NTD, DBD, linker, TET, and CTD are colored purple, blue, silver, green, and red, respectively. DNA is depicted as a black ribbon (a). The R175H mutation site is shown, highlighting its proximity to the zinc-coordination site (b). The zinc ion is shown as a purple sphere. The zinc-coordinating residues and the H175 residue are shown in licorice colored by atom type (C: cyan, O: red, N: blue, H: white).

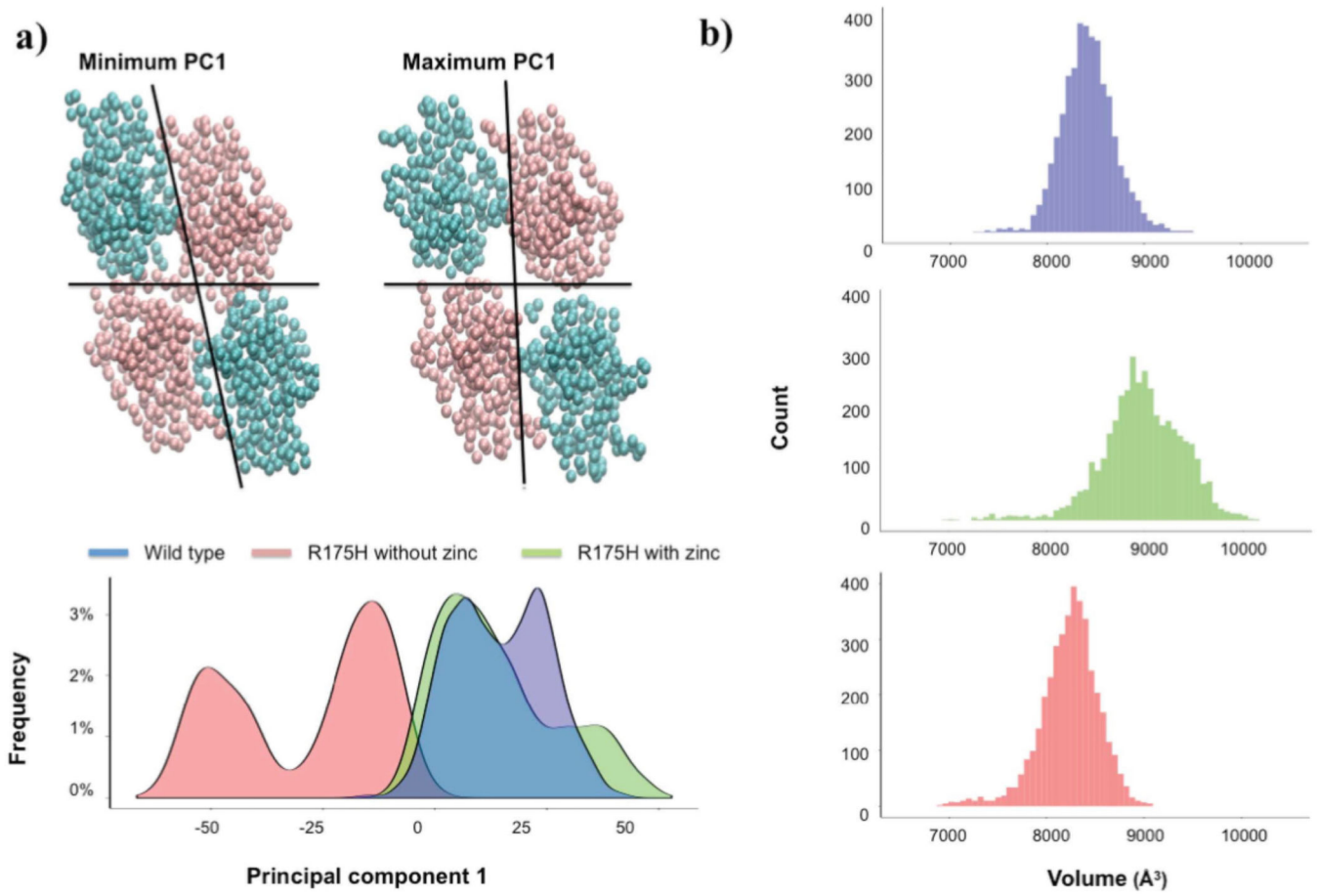

Figure 2.

Quaternary binding mode of the DNA binding domain in wild-type and R175H p53. The eigenvalues along PC1 are shown as a density plot for each fl-p53 system (a), where the asymmetric binding mode corresponds to low PC1 (R175H without zinc) and the symmetric binding mode corresponds to maximum PC1 (wild-type and R175H with zinc). The alpha carbons of the DBD for low and high PC1 are shown as spheres, where monomers A and D are colored cyan, and monomers B and C are colored pink. A histogram plot of the DNA grab volume is shown for all three fl-p53 systems (b).

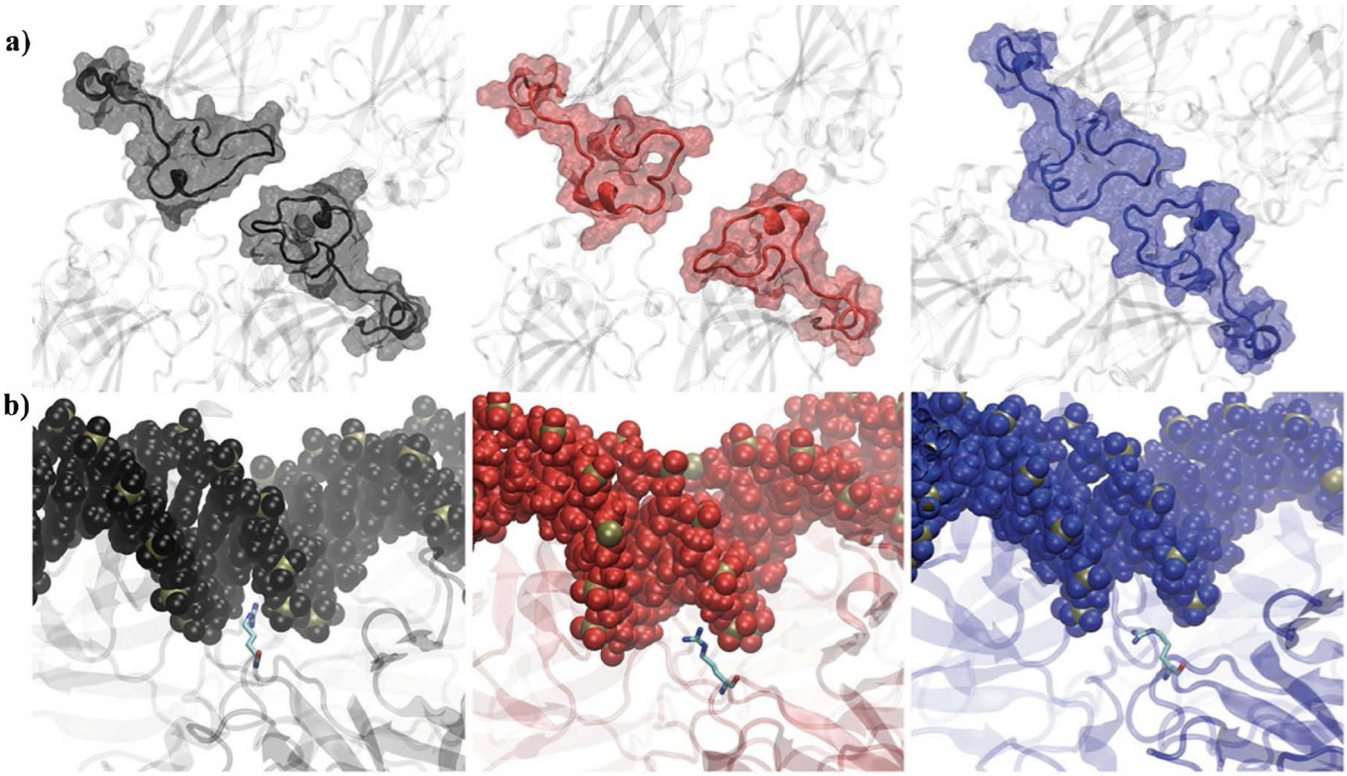

Figure 3.

Effects of R175H mutation and zinc loss on the L2 and L3 loops of p53 in the unique principal component conformations. The most-populated cluster representative frame for each fl-p53 system reveals differences in the L2 loop conformation (a) and the R248 residue conformation of the L3 loop (b). In (a), the L2 loop (residues 164–194) for wildtype, R175H with zinc, and R175H without zinc systems is shown as black, red, and blue ribbons and same-colored transparent surfaces, respectively, the rest of the protein is colored in silver ribbons. In (b), Arg248 is shown in sticks colored by atom type (H: white, C: silver, N: blue, O: red). The DNA for wildtype, R175H with zinc, and R175H without zinc systems is depicted in spheres colored black, red, and blue, respectively. Phosphate atoms in DNA are shown in tan for contrast. The p53 proteins are drawn as transparent ribbons colored according to the system as well.

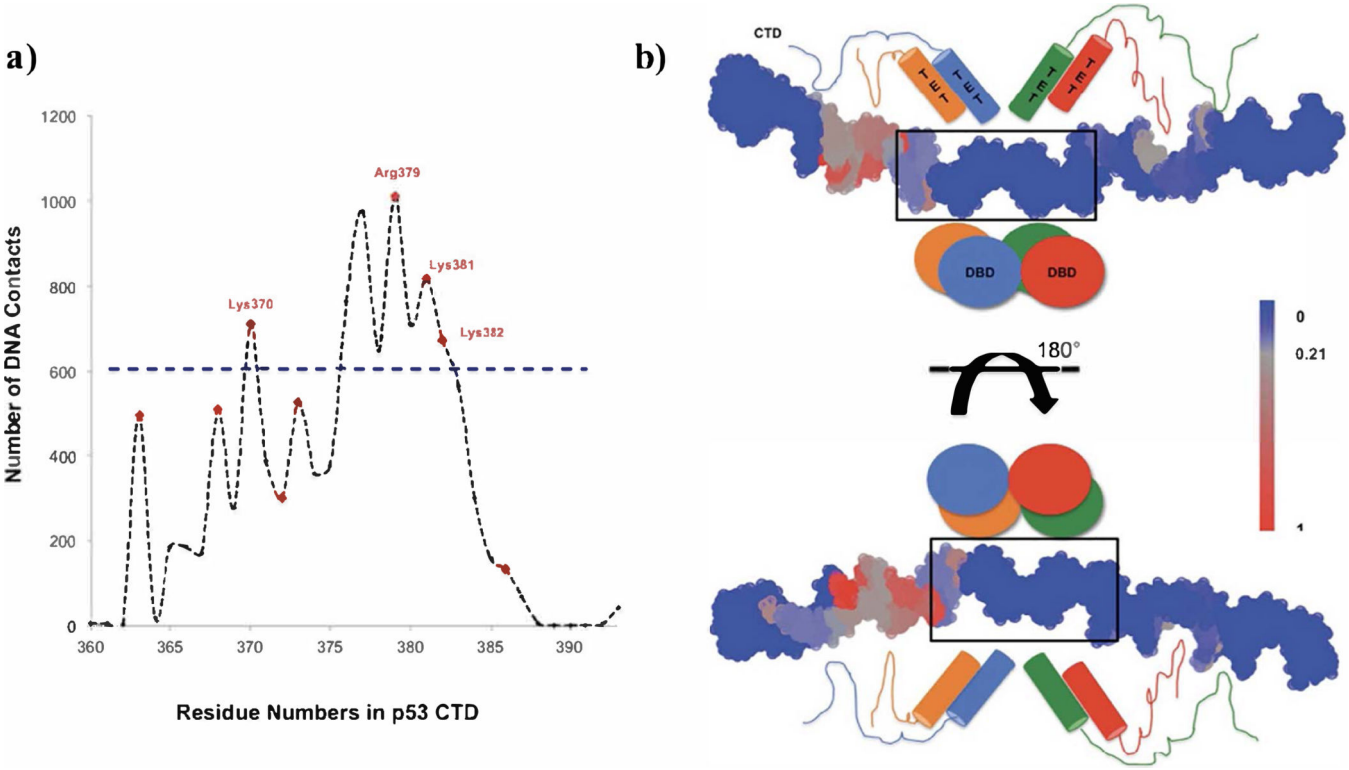

Figure 4.

Footprint analysis of the CTD-DNA contact residues averaged across all three p53 systems. The residues in the CTD that come within 3.5Å of the DNA were averaged across each monomer and all three p53 systems (a). The positively charged CTD residues are highlighted in red. A value cutoff for the number of DNA contacts formed of 600 is selected (dashed blue line) since it is at least half of the maximum CTD-DNA contacts. The four positively charged CTD residues that meet this cutoff are labeled. The same footprint analysis is done from the perspective of the DNA, in which the number of CTD contacts is mapped onto the DNA (b). The number of CTD contacts are normalized, ranging from 0 (no CTD contacts) to 1 (maximum number of CTD contacts). A cartoon of the DBD, TET, and CTD domains are depicted to highlight the orientation of the DNA, and the DNA response element is highlighted with a black box.

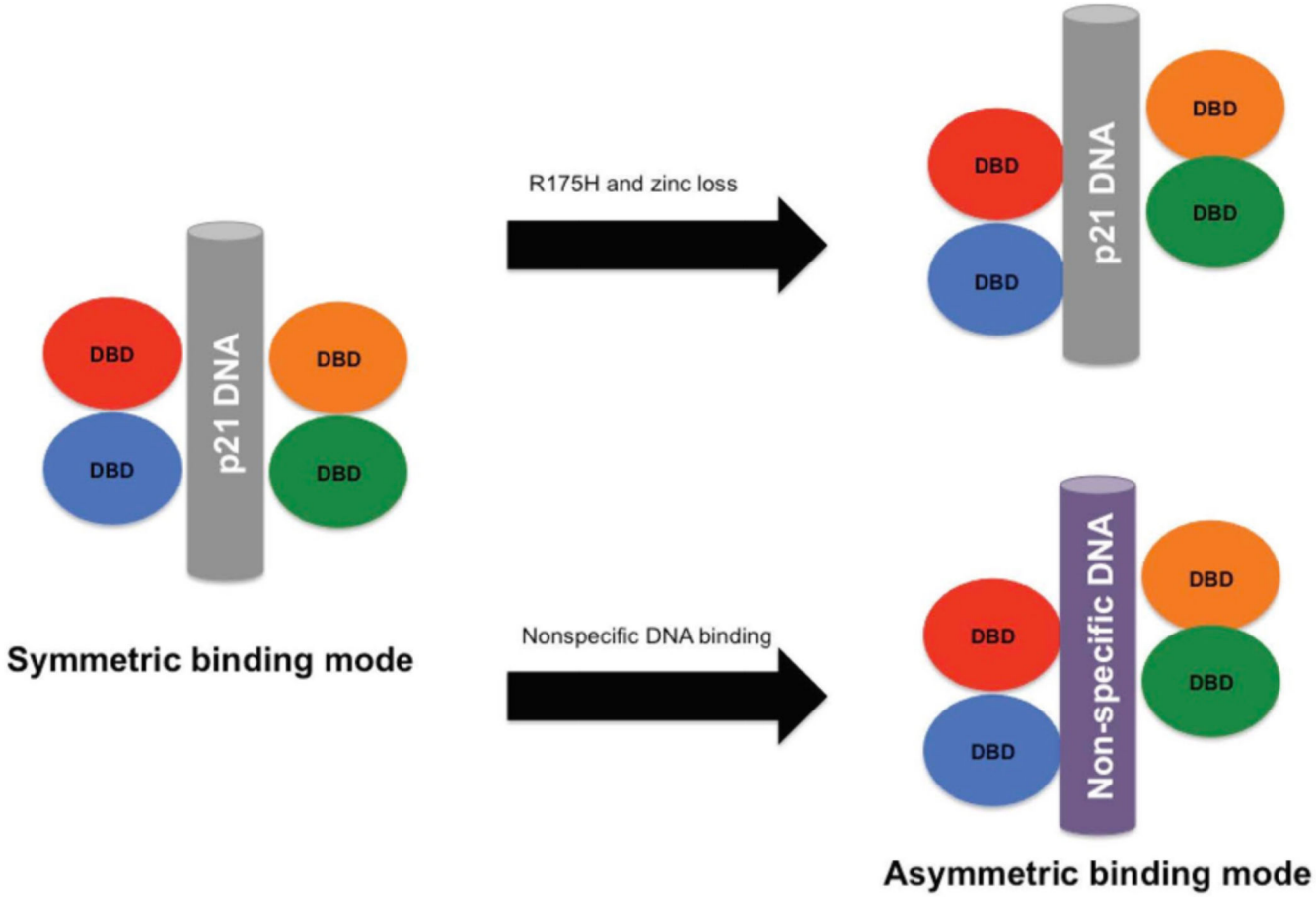

Figure 5.

DBD binding modes in p53 transcriptional activation. Under normal unstressed p53 conditions, the DBD is proposed to adopt a symmetric binding mode. Perturbation of p53 via the R175H mutation and zinc loss or nonspecific DNA binding shifts the DBD mode to an asymmetric conformation.

Table 1.

Hydrogen Bonding Interactions between L2 loops in Monomers B and C

Wild-type MD copy 1		
Monomer B L2 Residue	Monomer C L2 Residue	% interaction
186	183	0.05%
R175H without zinc MD copy 1		
184	183	39.6%
182	184	20.3%
182	183	11.4%
185	181	8.15%
183	183	3.55%